REPORT DOCUMENTATION PAGE

Form Approved
OMB No. 0704-0188

PLEASE DO NOT RETURN YOUR FORM TO THE ABOVE ORGANIZATION.

1. REPORT DATE *(DD-MM-YYYY)*	2. REPORT TYPE	3. DATES COVERED *(From - To)*
29-07-2014	Conference Proceeding	

4. TITLE AND SUBTITLE
Relationship Between Sea Surface Salinity from L-band Radiometer and Optical Features in the East China Sea

5a. CONTRACT NUMBER

5b. GRANT NUMBER

5c. PROGRAM ELEMENT NUMBER
0601153N

6. AUTHOR(S)
Bumjun Kil, Derek Burrage, Joel Wesson and Stephan Howden

5d. PROJECT NUMBER

5e. TASK NUMBER

5f. WORK UNIT NUMBER
73-4260-03-5

7. PERFORMING ORGANIZATION NAME(S) AND ADDRESS(ES)
Naval Research Laboratory
Oceanography Division
Stennis Space Center, MS 39529-5004

8. PERFORMING ORGANIZATION REPORT NUMBER
NRL/PP/7330--14-2132

9. SPONSORING/MONITORING AGENCY NAME(S) AND ADDRESS(ES)
Office of Naval Research
One Liberty Center
875 North Randolph Street, Suite 1425
Arlington, VA 22203-1995

10. SPONSOR/MONITOR'S ACRONYM(S)
ONR

11. SPONSOR/MONITOR'S REPORT NUMBER(S)

12. DISTRIBUTION/AVAILABILITY STATEMENT
Approved for public release, distribution is unlimited.

20140805590

13. SUPPLEMENTARY NOTES

14. ABSTRACT
The East China Sea (ECS) is often obscured from space in the visible and near-visible bands by cloud cover, which prevents remote sensing retrieval of optical properties. However, clouds are transparent to microwaves, and satellites with L-band radiometers have recently been put into orbit to monitor sea surface salinity (SSS). Previous studies have used the mixing of fluvial colored dissolved organic matter (CDOM) near coasts, where the mixing is approximately conservative over short time scales, to estimate SSS. In this study, the usual relationship between CDOM and salinity in the ECS has been used in reverse to estimate CDOM from remotely sensed SSS in the ECS and compare that CDOM with MODIS data. The SSS data used are 7 day composites from NASA's Aquarius/SAC-D satellite which has an L-band radiometer. The challenges in using this approach are that 1) Aquarius SSS has coarse spatial resolution (150 km), and 2) the ECS has numerous anthropogenic sources of radiofrequency interference which adds noise to the L-band signal for the SSS retrievals. Despite the limits in the method, CDOM distribution in the ECS can be estimated under cloudy conditions. In addition to all-weather retrievals, an additional advantage of the approach is that the algorithm provides an estimate of CDOM absorption that is unaffected by the spectrally similar detritus absorption that can confound optical remote sensing estimates of CDOM.

15. SUBJECT TERMS
East China Sea, sea surface salinity, colored dissolved organic matter, Aquarius/SAC-D

16. SECURITY CLASSIFICATION OF:			17. LIMITATION OF ABSTRACT	18. NUMBER OF PAGES	19a. NAME OF RESPONSIBLE PERSON
a. REPORT	b. ABSTRACT	c. THIS PAGE			Derek Burrage
Unclassified	Unclassified	Unclassified	UU	12	19b. TELEPHONE NUMBER *(Include area code)* (228) 688-5241

Relationship between sea surface salinity from L-band radiometer and optical features in the East China Sea

Bumjun Kil*[a], Derek Burrage[b], Joel Wesson[b] and Stephan Howden[a]
[a]Department of Marine Science, University of Southern Mississippi, Stennis Space Center, MS, USA;
[b]Naval Research Laboratory, Oceanography Division, Stennis Space Center, MS, USA

ABSTRACT

The East China Sea (ECS) is often obscured from space in the visible and near-visible bands by cloud cover, which prevents remote sensing retrieval of optical properties. However, clouds are transparent to microwaves, and satellites with L-band radiometers have recently been put into orbit to monitor sea surface salinity (SSS). Previous studies have used the mixing of fluvial colored dissolved organic matter (CDOM) near coasts, where the mixing is approximately conservative over short time scales, to estimate SSS. In this study, the usual relationship between CDOM and salinity in the ECS has been used in reverse to estimate CDOM from remotely sensed SSS in the ECS and compare that CDOM with MODIS data. The SSS data used are 7 day composites from NASA's Aquarius/SAC-D satellite which has an L-band radiometer. The challenges in using this approach are that 1) Aquarius SSS has coarse spatial resolution (150 km), and 2) the ECS has numerous anthropogenic sources of radiofrequency interference which adds noise to the L-band signal for the SSS retrievals. Despite the limits in the method, CDOM distribution in the ECS can be estimated under cloudy conditions. In addition to all-weather retrievals, an additional advantage of the approach is that the algorithm provides an estimate of CDOM absorption that is unaffected by the spectrally similar detritus absorption that can confound optical remote sensing estimates of CDOM.

Keywords: East China Sea, Sea surface salinity, Colored dissolved organic matter, Aquarius/SAC-D

1. INTRODUCTION

The East China Sea (ECS; mean depth <100 m), one of the largest marginal seas, extends from the southwestern area off Cheju Island to the northern area off Taiwan Island, and is bounded on the east by Japan and on the west by mainland China from which it receives the huge outflow from the Changjiang River (CR). Because of its large drainage basin, the CR contributes the majority of freshwater input to the coastal waters of China [1]. The CR plume spreads eastward over the broad ECS during the late spring through summer, reaching as far as Cheju Island and the shelf-break, where the Kuroshio Warm Current (KWC) flows northward to the Tsushima Strait [2]. This leads to extensive water exchange between the ECS and KWC across the shelf break through frontal and other oceanic processes [3]. Because the rivers are the main sources of colored dissolved organic matter (CDOM) in coastal regions, an inverse correlation between CDOM concentration and salinity can usually be found (i.e. CDOM is high where salinity is low) [4].

Since CDOM can be estimated from optical remote sensing [5], several empirical algorithms have been investigated, to retrieve sea surface salinity (SSS) from CDOM absorption at 400 nm, in the ECS [3, 6, 7]. However, there are two challenges for remote sensing of CDOM in the ECS. First, the ECS is well known to have frequent cloud cover, which hampers collecting optical features for particular seasons [19]. Secondly, because the absorption coefficient due to CDOM (a_g; i.e. gelbstoff) and non-algal particles (a_d; i.e. detritus) have similar spectral curves [8], under highly turbid conditions detritus can significantly affect, or even dominate the total light absorption and confound the retrieval of CDOM [9, 10]. The combined absorption due to detritus and gelbstoff (a_{dg}) is what is actually estimated from the satellite measurements. The a_d in the shelf waters of the ECS has been observed to be very high in the winter season [10] (Table 1). It has also been found that the ratio of a_d/a_{dg} can be greater than 0.1 in the regions close to estuaries and coasts, where the concentrations

Ocean Sensing and Monitoring VI, edited by Weilin W. Hou, Robert A. Arnone, Proc. of SPIE
Vol. 9111, 91110A · © 2014 SPIE · CCC code: 0277-786X/14/$18 · doi: 10.1117/12.2052951

of non-algal particles (e.g. suspended sediment) is higher than in the open ocean [8, 11]. Under these conditions, estimations of SSS from CDOM can be contaminated by detritus. The use of SSS to infer CDOM, based upon empirical relationships between *in situ* measured salinity and CDOM is a possible solution for estimating realistic CDOM under these conditions.

Until recently, with the exception of an experiment on Skylab in the 1970's [29], measuring SSS from L-band (1.4 GHz, 21 cm) radiometers were only used from aircraft. For example, measurements of SSS using the Salinity, Temperature and Roughness Remote Scanner (STARRS), over Mobile Bay and Mississippi Sound [12, 13], have been compared with SSS estimates derived from optically-sensed CDOM in Louisianan coastal waters [14, 15]. In the East China Sea, it was pointed out in 2004 that CDOM could be estimated from SSS using the Scanning Low-Frequency Microwave Radiometer (SLFMR - predecessor to STARRS) flown on an aircraft [6]. Currently there are two satellites with L-band radiometers, in orbit about the earth for measuring SSS. There is the Aquarius/SAC-D satellite [16], which is operated by NASA, and the Soil Moisture and Ocean Salinity (SMOS) satellite operated by the European Space Agency (ESA). In the East China Sea, data from the Aquarius/SAC-D satellite (here after referred to as Aquarius) is available as a level3 (L3).

Table 1. The previously studied $a_g(440)$ and $a_d(440)$ [10]. The $a_g(400)$ was approximated from $a_g(440)$ (Spectral slope: 0.017nm^{-1}; LEI Hui et al., 2012) using exponential decay function [20, 21, 22] to be employed as a reference value in this research.

Season	Mid shelf		Outer Shelf		Approximated $a_g(400)$	
	$a_g(440)$	$a_d(440)$	$a_g(440)$	$a_d(440)$	Mid shelf	Outer Shelf
Summer	0.070±0.047m^{-1}	0.005±0.005m^{-1}	0.051±0.031m^{-1}	0.004±0.005m^{-1}	0.138±0.093m^{-1}	0.10±0.061m^{-1}
Winter	0.037±0.018m^{-1}	0.052±0.045m^{-1}	0.025±0.014m^{-1}	0.004±0.002m^{-1}	0.073±0.035m^{-1}	0.049±0.028m^{-1}

However, it is challenging to estimate SSS from Aquarius in marginal seas, and the ECS in particular, for two reasons: First, SSS is negatively biased in this region due to persistent low levels of Radio Frequency Interference (RFI) from the coastal areas (e.g. North Atlantic and Asia-Pacific regions), despite the process of RFI filtering in the L3 processing [17].

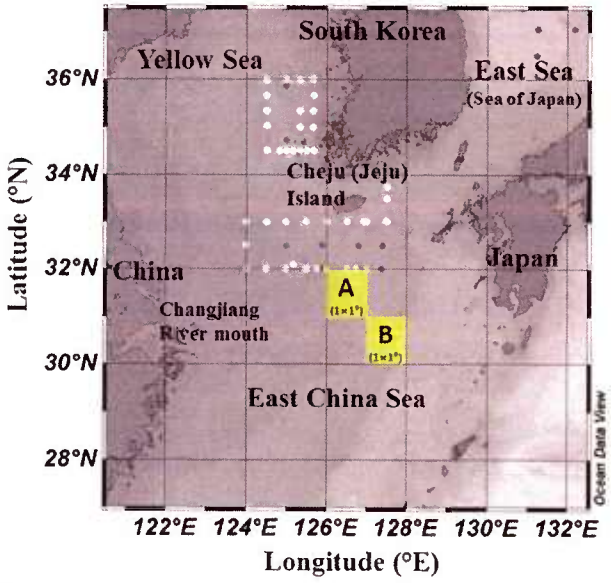

Figure.1 The map of data collection and time series analysis area (A: Mid shelf, B: Outer shelf) for MODIS and Aquarius data. The white colored dots represent the *in situ* SSS and optical data from SeaBASS, the gray colored dots are the *in situ* SSS from KODC which are collocated with single pixel of Aquarius SSS.

Secondly, the coarse spatial resolution (~150 km) and long revisit time (3 days or more) of Aquarius [16] is not as optimal for coastal and marginal seas applications as is ocean color, such as from the Aqua MODIS satellite [7].

2. DATA AND ANALYSIS

The SSS data used is the 7 days composite L3 V.2 data from Aquarius, and it was acquired from the Physical Oceanography Distributed Active Archive Center (PODAAC) at http://podaac.jpl.nasa.gov/SeaSurfaceSalinity/Aquarius. We retrieved Aqua-MOIDS 8 days composite remote sensing reflectance at 412, 555 nm (Rrs412, Rrs555) and absorption coefficient due to detritus and gelbstoff at 443 nm ($a_{dg}(443)$), available as level 3 production (QAA algorithm [28]), via MODIS Ocean Color Web [23] at http://oceancolor.gsfc.nasa.gov. *In situ* SSS and absorption coefficient due to gelbstoff at 400nm ($a_g(400)$) were collected by the National Fisheries Research and Development Institute (NFRDI) and were downloaded from the Korea Oceanographic Data Center (KODC) at http://kodc.nfrdi.re.kr. Sixty annual stations in the coastal region around the Korean Peninsula [24] were collocated with Aquarius pixels. These collocated SSS from Aquarius and NFRDI were employed to correct the bias in Aquarius SSS (Table 2). In order to select the algorithms to estimate $a_g(400)$ from SSS ($a_g(400)_{SSS}$), we obtained 39 observations of *in situ* $a_g(400)$ and SSS in the Yellow Sea and the southern area of Cheju Island collected by GEO-CAPE and GOCI mission via SeaWiFS Bio-optical Archive and Storage System (SeaBASS; available at http://seabass.gsfc.nasa.gov/) [25] (Table 2; Figure1).

Table 2. The lists of ship board (situ) and remote sensing measurement (satellite) in this research.

Measurement	Mission	Data	Dates of observation
Ship board (*In situ*)	NFRDI annual cruise (Stored in KODC)	SSS which were collocated with Aquarius pixels (< 0.5 deg / 60 EA)	2012.02.03 - 11. 29
	GEO-CAPE and GOCI (Stored in SeaBASS)	$a_g(400)$, SSS (39 EA)	2010.11.30 - 12.01 2011.04.15 - 04.17 2011.08.10 -08.12
Remote sensing (satellite)	NASA Aquarius/SAC-D	SSS L3 V.2 (7 days)	2012.02.03 - 11. 29
	NASA Aqua MODIS	Rrs(555), Rrs(412), $a_{dg}(443)$ / 8 days	2012.02.03 - 11. 29

We evaluated (reversed) algorithms for $a_g(400)_{SSS}$ from previous studies by superimposing with the plot of *in situ* $a_g(400)$ and SSS. For this study, that uses CDOM absorption from MODIS at 400 nm, the previously published data for $a_g(440)$ and $a_d(440)$ [10] in table 1, were converted to $a_g(400)$ using an exponential decay function [20, 21, 22]. The process shown in figure 2 was used to produce $a_g(400)_{SSS}$ from Aquarius SSS. First a bias correction is made by comparing Aquarius SSS with *in situ* SSS. Because the bias of Aquarius SSS has seasonal differences [17], we selected a particular season for which bias is at a minimum. The geometric mean (GM) regression method [26] is employed to correct the negative bias of Aquarius SSS by comparing with *in situ* SSS from KODC. Next the bias corrected SSS is used in an inverted transformation of one of the published algorithms for deriving SSS from $a_g(400)$. The resultant $a_g(400)$ is mapped horizontally and compared with maps of $a_g(400)$ from MODIS ($a_g(400)_{MODIS}$). We estimated $a_g(400)_{MODIS}$ based on Moon et al (2010)'s algorithm [27] : $a_g(400) = 0.2355 \times (Rrs412/Rrs555)^{-1.3423}$. The resulting $a_g(400)$ may have pixels which are contaminated by absorption due to detritus. These pixels were identified by finding a threshold on $a_{dg}(443)$, which corresponds approximately to $a_d(443) = 0.1 \times a_{dg}(443)$ based on open ocean (case 1 waters) [9, 11]. Once the threshold was determined (see below), the pixels of $a_g(400)$ containing high $a_d(443)$ values were identified and eliminated to produce a data set with less contamination due to detritus (i.e. remaining detritus free $a_g(400)_{MODIS}$).

Finally, we evaluated both $a_g(400)_{Aqs}$ and $a_g(400)_{AqsCorr}$ by comparing them with detritus free $a_g(400)_{MODIS}$. The comparisons were done for both time series and spatial maps. Time series comparisons were done over two different areas. The first area, area A (Figure 1), is characterized by turbid conditions on the shelf in depths of 50 - 100 m. The second area, area B (Figure 1), is characterized by less turbid in deeper waters of 100 - 500 m depths. Comparison of spatial maps, over one time period, was done for $a_g(400)_{Aqs}$, $a_g(400)_{AqsCorr}$, and detritus free $a_g(400)_{MODIS}$ (Figure 1).

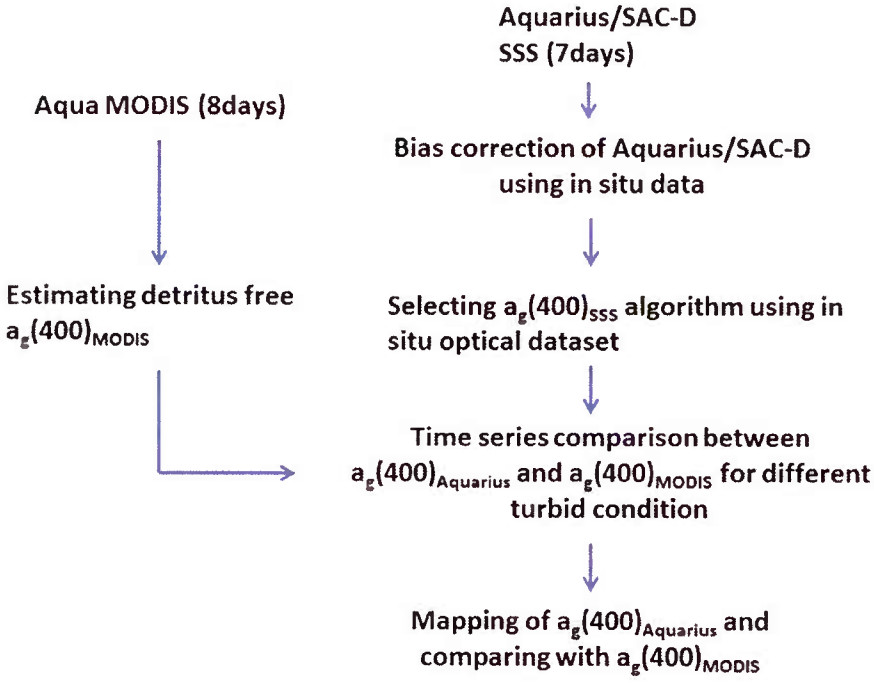

Figure 2. The overall work process in this research to estimate and evaluate $a_g(400)_{SSS}$ from Aquarius.

3. RESULT

3.1 Production of $a_g(400)_{AqsCorr}$

3.1.1. Correcting bias in Aquarius

As stated in a previous report [17], the mean difference between Aquarius SSS and *in situ* SSS (ΔSSS) is negative. In order to avoid severe contamination due to unfiltered RFI, we selected the Fall-winter season (September 2 - November 29, 2012) which shows a relatively low bias (Figure 3a). Subsequently, we compared the selected 17 collocated pixels of Aquarius SSS with *in situ* SSS (< 0.5 deg) during that season. As shown in figure 3b, most Aquarius SSS showed a negative biased from the *in situ* SSS. To correct the bias, we established the equation to correct the original Aquarius SSS (SSS_{Aqs}) as an input source, and corrected one ($SSS_{AqsCorr}$) as an output product by inverting the original equation obtained by GM regression of Aquarius SSS with the *in situ* data [26] (i.e. SSS_{Aqs} = 1.2357 × *in situ* SSS - 8.4621) as a following equation (Figure 3b).

$$SSS_{AqsCorr} = 0.8092 \times SSS_{Aqs} + 6.8479. \quad (1)$$

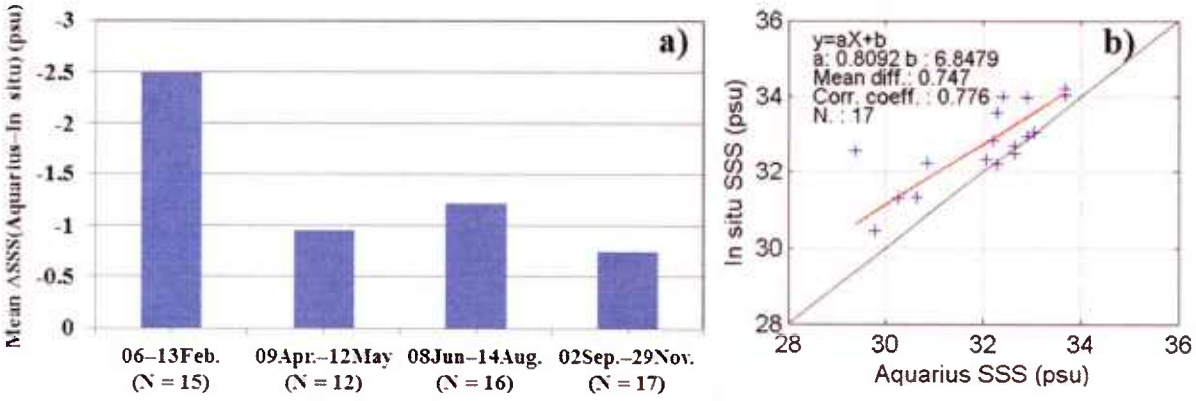

Figure 3. a) The histogram represents the seasonal mean ΔSSS (Aquarius minus *in situ* SSS), b) The relation between *in situ* and Aquarius SSS in the September 2 – November 29 in 2012 which was selected in Figure 3a, the trend line represents the equation by GM regression.

The SSS time series in areas A and B are shown in figure 4, along with the SSS corrected using Equation 1. The corrected SSS (blue colored solid line with star) in area A is reflecting coastal water (< 34 psu) (Figure 4a). Area B shows offshore saline condition of KWC [3] (≥ 34 psu) at times (Figure 4b).

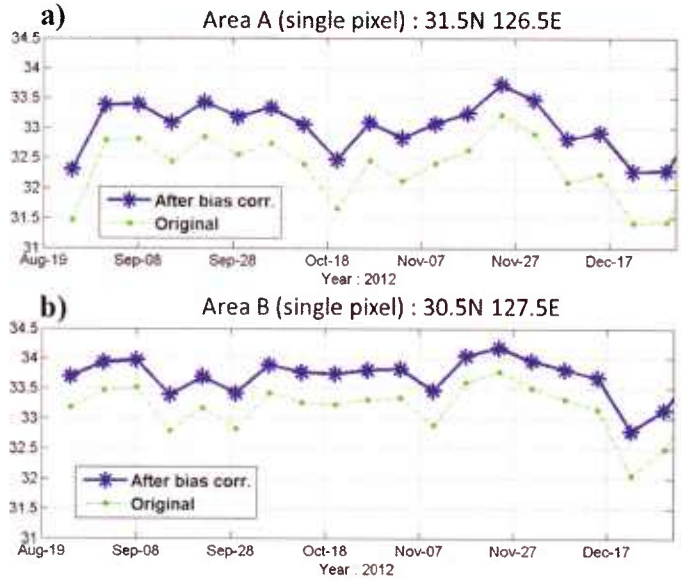

Figure 4. Time series plot of Aquarius SSS (blue colored solid line with star : bias corrected SSS, green colored dashed line with dot : original SSS) in the Fall – Winter in 2012, the red solid line is the official minimum of Aquarius SSS [16].

3.1.2. Selecting $a_g(400)_{SSS}$ algorithm for Aquarius

We selected three algorithms from Bai et al. (2013) [7] and Gong (2004) [6] which seasonally represent the relation between $a_g(400)$ and SSS. Because Bai et al.'s algorithm (Cruise 908 (C908), and Cruise 973 (C973)) were established to estimate SSS from optical remote sensing of $a_g(400)$, for this research the equations were simply inverted to estimate $a_g(400)$ from SSS (Table 3). Each algorithm has different regional coverage. C908 of Bai et al.(2013) [7] was developed for the CR

dominated region (inner shelf), and C973 of Bai et al (2013) [7] was developed for the offshore region including CR effects (inner + mid shelf). The algorithm of Gong (2004) [6] : was developed for the southwestern region of the ECS.

Table 3. The list of algorithms between SSS and $a_g(400)$ from previous studies in ECS.

Researcher	Equation	R^2	N	Range of $a_g(400)$
				Range of SSS
C908 : Bai et al.(2013)	$a_g(400)_{sss}$ = -0.02887×SSS+1.084303	0.92	264	0.0877 – 1.0823 m^{-1}
				34.52–0.07 psu
C973 : Bai et al.(2013)	$a_g(400)_{sss}$ = -0.04524×SSS+1.587794	0.81	163	0.0215 – 0.4689m^{-1}
				34.62–24.73 psu
Gong, 2004	$a_g(400)_{sss}$ = -0.033×SSS+1.209	0.78	137	0.017 – 0.444 m^{-1}
				36.12–23.18 psu

The three different algorithms were applied over the salinity range of the *in situ* SSS and plotted over the scatter plot of *in situ* $a_g(400)$ and SSS (Figure 5) obtained from the 28 casts taken from the mid shelf around South Cheju Island. The algorithm C973 of Bai et al (2013) [7] (red solid line) was selected since it is statistically closer to the data (i.e. low mean difference and RMSE). Using the C973 algorithm (Table 3), the algorithm of $a_g(400)$ from Aquarius ($a_g(400)_{Aqs}$) is:

$$a_g(400)_{Aqs} = f_{C973}(SSS_{Aqs})$$

$$= -0.04524 \times SSS_{AqsCorr} + 1.587794 \quad (2)$$

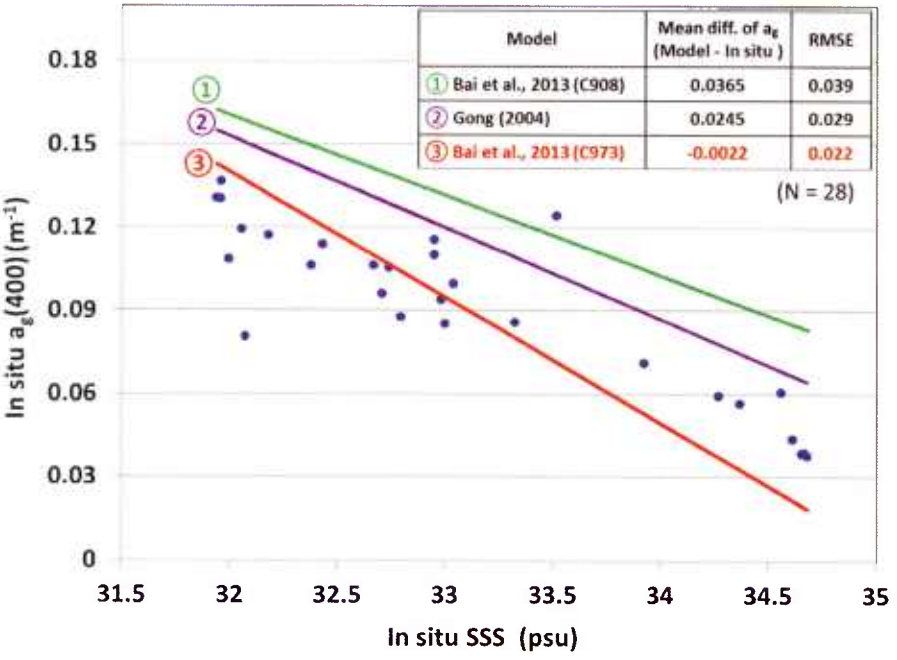

Figure 5. The algorithms which are superimposed over the scatter plots between *in situ* SSS and $a_g(400)$ in ECS from SeaBASS. The circled green "one": C908 of Bai et al.(2013) [7], the circled purple "two" : Gong (2004) [6], the circled red "three" : C973 of Bai et al(2013) [7].

3.1.3. Estimation of detritus free $a_g(400)_{MODIS}$

As shown in Figure 6, there are three pixels of $a_g(400)_{MODIS}$ which are close to the *in situ* measurements over the Yellow Sea and the southern Cheju Island. The other $a_g(400)_{MODIS}$ pixels were greatly overestimated relative to *in situ* measurements (several pixels were excluded due to exceedingly overestimated $a_g(400)_{MODIS}$). The figure shows that those overestimates of $a_g(400)$ from MODIS are associated with high $a_{dg}(443)$ ($> 0.04\ m^{-1}$), indicating contamination by detritus. This threshold in $a_{dg}(443)$ can be used to approximate a threshold for $a_d(443)$ at $0.004\ m^{-1}$, which is similar with previously published $a_d(440)$ in the outer shelf (Table1). Therefore, in this research, we empirically determined the threshold of $a_{dg}(443)$ as $0.04\ m^{-1}$ to remove the overestimated $a_g(400)_{MODIS}$ values.

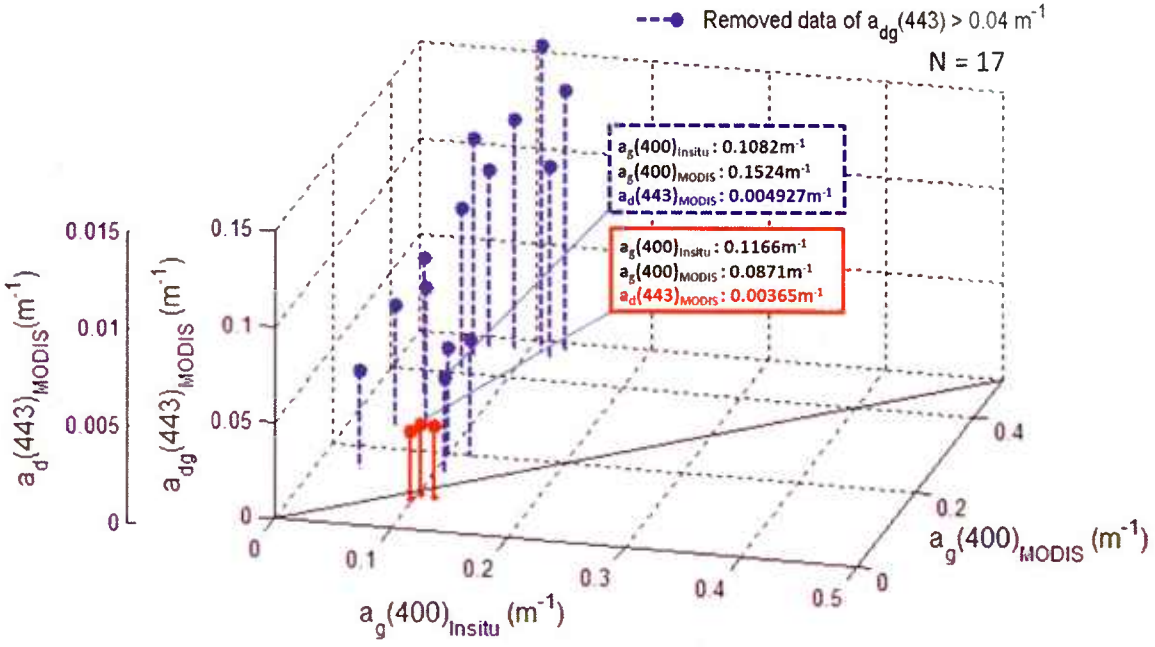

Figure 6. The stem plot of $a_g(400)_{In\ situ}$ and $a_g(400)_{MODIS}$ with $a_{dg}(400)_{MODIS}$. Z-axis farther left hand side represents $a_d(443)$ approximated as $0.1 \times a_{dg}(443)$ to compare previously published $a_d(440)$ [10] at table1. The blue dashed line stem is empirically removed data of which $a_{dg}(400)_{MODIS}$ is $> 0.04\ m^{-1}$ (i.e., likely contaminated by absorption due to detritus).

3.2. Evaluation of $a_g(400)_{AqsCorr}$

3.2.1. Time series evaluation

$a_g(400)_{AqsCorr}$ was estimated by inputting $SSS_{AqsCorr}$ into Equation 2, which was selected for the middle and outer shelf in ECS. In order to evaluate the improvement of $a_g(400)_{AqsCorr}$ over $a_g(400)_{Aqs}$, time series were plotted for the middle (area A) and outer (area B) shelves, along with detritus free $a_g(400)_{MODIS}$ for the fall-winter season in 2012 (Figure 7). There is a positive bias in $a_g(400)_{Aqs}$ (dashed line with cyan colored dot) relative to $a_g(400)_{MODIS}$ for both middle and outer shelves, which is greatly reduced for $a_g(400)_{AqsCorr}$ (solid line with blue colored star). The mean $a_g(400)_{AqsCorr}$ was closer to the MODIS mean (red bar) for both areas. Consequently, the bias correction of Aquarius SSS improved the estimates of CDOM absorption. However, although the means of $a_g(400)_{AqsCorr}$ are closer to the mean of $a_g(400)_{MODIS}$, the variation about the mean for $a_g(400)_{AqsCorr}$ matches $a_g(400)_{MODIS}$ better in area A on the mid shelf area, than it does in area B on the outer shelf. Thus, more work needs to be done to improve the estimates of $a_g(400)_{AqsCorr}$ in the outer shelf.

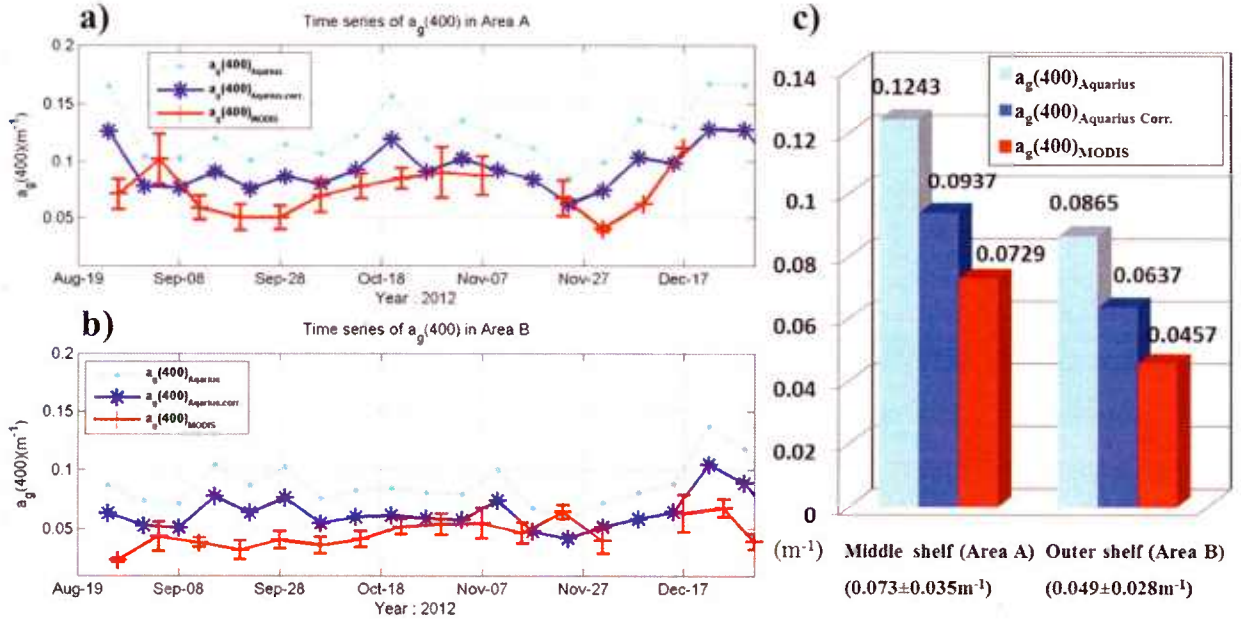

Figure 7. Time series plot of CDOM absorption, cyan dot dashed line: $a_g(400)_{Aqs}$, blue star solid line : $a_g(400)_{AqsCorr}$, red dashed line : $a_g(400)_{MODIS}$ (the bar represents standard deviation of the $a_g(400)_{MODIS}$ for the a) area A (Mid shelf) and b) Area B (Outer shelf)). c) The histogram of mean $a_g(400)$ in order of $a_g(400)_{Aqs}$, $a_g(400)_{AqsCorr}$, and $a_g(400)_{MODIS}$ for Area A (Mid shelf) and Area B (Outer shelf). The values at the bottom of the histogram are the mean and standard deviations for $a_g(400)$ in table1.

3.2.2. Spatial evaluation

The horizontal distribution of $a_g(400)$ was plotted to check the improvement from the bias correction of Aquarius by comparing with MODIS. The periods of October 28 - November 3, 2012 for Aquarius and October 31 - November 7, 2012 for MODIS were selected for mapping because that period had the lowest differences for both middle and outer shelf in the time series comparisons in figure 7a and 7b. The $a_g(400)_{AqsCorr}$ has lower values than $a_g(400)_{Aqs}$ (see gray dashed line in the figures 8a and 8b) and the features are similar looking to those of $a_g(400)_{MODIS}$. Specifically, the $a_g(400)_{AqsCorr}$ in the southeast off of Cheju Island has a feature in $a_g(400)_{AqsCorr}$ of less than $0.1m^{-1}$ which has been found to be a typical feature of the KWC [3].

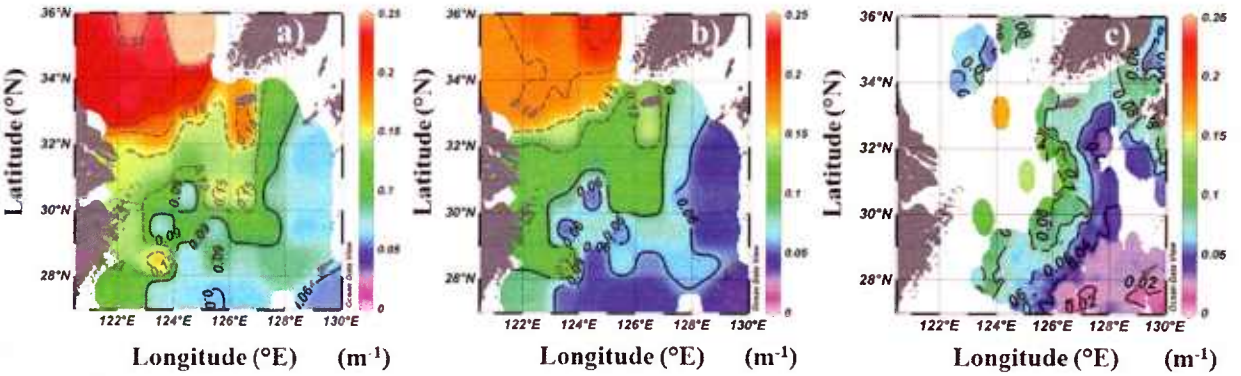

Figure 8. The horizontal distribution of a) $a_g(400)_{Aqs}$, b) $a_g(400)_{AqsCorr}$ in October 28 - November 3, 2012, c) $a_g(400)_{MODIS}$ in October 31 - November 7, 2012. The gray dashed line represents $a_g(400) \geq 0.12m^{-1}$.

In addition, the $a_g(400)_{Aqs}$ which has values higher than 0.15 m^{-1} in the center of ECS (Figure 8a) is reduced for $a_g(400)_{AqsCorr}$ (See the gray dashed line in figure 8a and 8b). Although $a_g(400)_{AqsCorr}$ is larger than $a_g(400)_{MODIS}$ in outer shelf, this might be due to the coarse resolution of Aquarius, which cannot catch smaller features in $a_g(400)$ that MODIS can resolve. Figure 9a shows locations where $a_g(400)_{MODIS}$ is collocated with $a_g(400)_{Aqs}$ and $a_g(400)_{AqsCorr}$. Scatter plots of the collocated $a_g(400)_{MODIS}$ with $a_g(400)_{Aqs}$, and $a_g(400)_{AqsCorr}$ are shown in figures 9b and 9c, respectively. The scatter plot in figure 9b shows a larger bias and more scatter than that in figure 9c. Moreover, the reduced average of $a_g(400)_{AqsCorr}$ (Figure 9c) satisfies the range of previously published $a_g(400)$ in the winter (Mid shelf : $0.073 \pm 0.035 m^{-1}$, Outer shelf : 0.049 ± 0.028 m^{-1}; see table 1) rather than $ag(400)_{Aqs}$. Consequently, the results shown above emphasize the importance of correcting biased SSS in Aquarius.

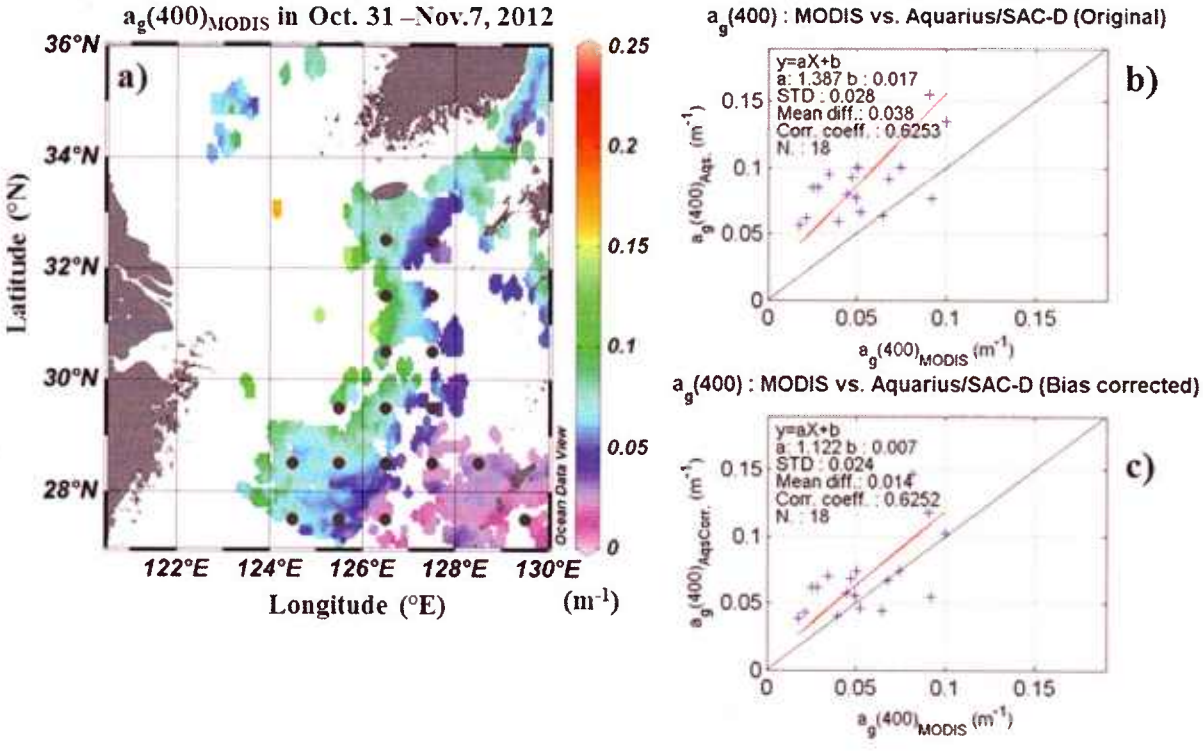

Figure 9. a) The collocated positions of $a_g(400)_{MODIS}$ and $a_g(400)_{Aqs}$ (Gray dots) over the $a_g(400)_{MODIS}$ (See Figure 8c), the regression plot between b) $a_g(400)_{Aqs}$ and $a_g(400)_{MODIS}$, c) $a_g(400)_{AqsCorr}$ and $a_g(400)_{MODIS}$, the blue cross scatters are from gray dots in Figure 9a.

4. Conclusion

Estimation of CDOM from remotely sensed SSS was attempted in order to collect optical features of the ECS under conditions of cloud cover and turbid conditions where absorption due to detritus can affect apparent CDOM absorption. This study has made three significant advances: First, a method was developed to check and correct for bias in Aquarius retrievals of SSS, presumably due to unfiltered RFI. Secondly, the selection of the most appropriate published algorithm relating SSS with CDOM for the middle and outer shelf in ECS was done. Lastly, a method for estimating detritus free CDOM from MODIS was developed and applied.

The Fall-Winter season of 2012 was selected because of the relatively low bias during that season. The bias was then corrected for using an empirical approach. Subsequently, we selected the previously published algorithm for SSS from $a_g(400)$ that best fit the observations ("C973all" cruise data by Bai et al.(2013) [7]) . We estimated detritus free CDOM by empirically matching the relation between $a_g(400)_{In\ situ}$ and $a_g(400)_{MODIS}$ with $a_{dg}(443)_{MODIS}$ using previously published a_d/a_{dg} ratios in order to remove detritus contaminated $a_g(400)_{MODIS}$. The $a_g(400)_{Aqs}$ and $a_g(400)_{AqsCorr}$ were estimated by inputting SSS_{Aqs} and $SSS_{AqsCorr}$, respectively into the inverted algorithm of Bai et al.(2013) from the C973 cruise. These were then compared with detritus free $a_g(400)_{MODIS}$.

Accordingly, $a_g(400)_{AqsCorr}$ better matched $a_g(400)_{MODIS}$ than did $a_g(400)_{Aqs}$. Despite the coarse spatial resolution of the Aquarius data, relative to MODIS, $a_g(400)_{AqsCorr}$ showed similar patterns to $a_g(400)_{MODIS}$ where cloud free areas exist, over the high turbid mid shelf in the fall-winter season. Consequently, this approach is shown to be useful to provide information on CDOM in the ECS from L-band radiometry. Although this study demonstrated that Aquarius data is useful for obtaining optical features in the ECS using passive microwave remote sensing, further application of the higher spatial resolution data (30 – 50 km) from the L-band radiometer on SMOS satellite [18], combined with its shorter revisit time (~3 days) should be investigated in the future.

5. Acknowledgment

The Aquarius/SAC-D data was provided by NASA Jet Propulsion Laboratory via Physical Oceanography Distributed Active Archive Center. The Aqua-MODIS data was provided via NASA Ocean color web. The KODC *in situ* salinity data was provided by Republic of Korea National Fisheries Research and Development Institute. The authors would like to thank Dr. Antonio Mannino in NASA Goddard Space Flight Center for providing the CDOM measurement, Dr. Se-Jong, Ju in Korea Institute of Ocean Science and Technology for providing ocean salinity measurement in the East China Sea via NASA SeaWiFS Bio-optical Archive and Storage System. The first author would like to thank Dr. Jerry Wiggert and Robert Arnone in the University of Southern Mississippi for good suggestions. And the first author gratefully acknowledges receipt of a student travel grant awarded by Society of Photographic Instrumentation Engineers. Work by the second and third author was supported by the Office of Naval Research as part of NRL's basic research project Sea Surface Roughness Impacts on Microwave Sea Surface Salinity Measurements (SRIMS) under Program Element 61153N. This is NRL contribution NRL/PP/7330-14-2132.

REFERENCE

[1] Guo, Z., Lin, T., Zhang, G., et al., "The sedimentary fluxes of polycyclic aromatic hydrocarbons in the Yangtze River Estuary coastal sea for the past century," Science of The Total Environment, 386, 33-41(2007).

[2] Lie, H. J., Cho, C. H., Lee, J. H., et al., "Structure and eastward extension of the Changjiang River plume in the East China Sea, " J. Geophys. Res., 108(C3), 3077(2003), doi:10.1029/2001JC001194.

[3] Ahn, Y. H., Shamugam, P., Moon, J.E., et al., "Satellite remote sensing of a low-salinity water plume in the East China Sea," Annales Geophysicae, Copernicus GmbH, 26(7), (2008).

[4] Blough, N.V., and Del Vecchio, R., Chromophoric DOM in the coastal environment, Biogeochemistry of Marine Dissolved Organic Matter,D.A. Hansell and C.A. Carlson, eds., Academic Press, Cambridge, 509-546 (2002).

[5] Coble, Paula, et al., "Colored Dissolved Organic Matter in the Coastal Ocean: An Optical Tool for Coastal Zone Environmental Assessment & Management," No. NRL/JA/7330-04-15. NAVAL RESEARCH LAB STENNIS SPACE CENTER MS OCEANOGRAPHY DIV (2004).

[6] Gong, G.C., "Absorption coefficients of colored dissolved organic matter in the surface waters of the East China Sea," Terrestrial Atmospheric and Oceanic Sciences 15(1), 75-88 (2004).

[7] Bai, Yan, et al. "Remote sensing of salinity from satellite-derived CDOM in the Changjiang River dominated East China Sea," Journal of Geophysical Research: Oceans 118(1), 227-243(2013).
[8] Roesler C. S., Perry M. J., and Carder K L., "Modeling in situ phytoplankton absorption from total absorption spectra in productive inland marine waters," Limnology And Oceanography, 34(8), 1510–1523 (1989).
[9] Shen, F., Zhou, Y., and Hong, G., "Absorption Property of Non-algal Particles and Contribution to Total Light Absorption in Optically Complex Waters, a Case Study in Yangtze Estuary and Adjacent Coast," Advances in Computational Environment Science. Springer Berlin Heidelberg, 61-66 (2012).
[10] LEI Hui, et al. "The proportions and variations of the light absorption coefficients of major ocean color components in the East China Sea." Acta Oceanologica Sinica 31(2),45-61 (2012).
[11] Zhu, Weining, et al. "Estimation of chromophoric dissolved organic matter in the Mississippi and Atchafalaya river plume regions using above-surface hyperspectral remote sensing." Journal of Geophysical Research: Oceans (1978–2012) 116.C2 (2011).
[12] Droppleman, J. D., R. A. Mennella, and D. E. Evans. "An airborne measurement of the salinity variations of the Mississippi River outflow." Journal of Geophysical Research 75(30), 5909-5913 (1970).
[13] Burrage, D., Miller, J., Johnson, D.,J., et al., "Observing sea surface salinity in coastal domains using an airborne surface salinity mapper". Presented at OCEANS'02 MTS/IEEE , 4, 2014-2024 (2002b).
[14] Wesson, J.C, Burrage, D.M., Maisonet, V.J., et al, "Aircraft and in-situ salinity and ocean color measurement and comparison in the Gulf of Mexico," Geoscience and Remote Sensing Symposium 2008, IGARSS 2008. IEEE International, 4, 383-386 (2008).
[15] Maisonet, V. J., Wesson, J., Burrage, D., and Howden, S.,"Measuring coastal sea surface salinity of the Louisiana shelf from aerially observed ocean color", IEEE, 1-4 (2009).
[16] Lagerloef, G., et al., "The Aquarius/SAC-D mission: Designed to meet the salinity remote-sensing challenge, " Oceanography, 21, 68–81(2008), doi:10.5670/oceanog.2008.68.
[17] Lagerloef, G., H.Y. Kao, O. Melnichenko, P. Hacker, E. Hackert, and Y. Chao, "Aquarius salinity validation analysis," Aquarius Project Document: AQ-014-PS-0016, 18, (2013).
[18] Y. H. Kerr, Waldteufel, P., Wigneron, J. P., et al., "The SMOS mission: New tool for monitoring key elements of the global water cycle," Proc. IEEE 98(5), 666–687(2010).
[19] He, X., Bai, Y., Pan, D., et al."Satellite views of the seasonal and interannual variability of phytoplankton blooms in the eastern China seas over the past 14 yr (1998–2011)". Biogeosciences, 10, 4721–4739 (2013)
[20] Yentsch C S., "Measurement of visible light absorption by particulate matter in the ocean," Limnology and Oceanography, 7(2), 207–217 (1962).
[21] Bricaud A, Morel, A., Babin, M., et al., "Variations of light absorption by suspended particles with chlorophyll a concentration in oceanic (Case 1) waters: analysis and implications for bio-optical models," J Geophys Res, 103(C13): 31033–31044 (1998).
[22] Prieur, L., and Sathyendranath, S., "An optical classification of coastal and oceanic waters based on the specific spectral absorption curves of phytoplankton pigments, dissolved organic matter, and other particulate materials," Limnol Oceanogr, 26(4), 671–689 (1981).
[23] Feldman, G. C., and McClain, C. R.,"Ocean Color Web, MODIS Reprocessing L3 of Rrs412,Rrs555,adg(443), " NASA Goddard Space Flight Center. Eds. Kuring, N., Bailey, S. W., (1April, 2014), http://oceancolor.gsfc. nasa.gov/.
[24] Korea Oceanographic Data Center, "Newsletter No.1," Korea Oceanographic Data Center National Fisheries Research and Development Institute (NFRDI) (in Korean) (1984).
[25] P.J. Werdell and Bailey, S.W., "The SeaWiFS Bio-optical Archive and Storage System (SeaBASS): Current architecture and implementation," NASA Tech. Memo. 2002-211617 , G.S. Fargion and C.R. McClain, Eds., NASA Goddard Space Flight Center, Greenbelt, Maryland, 45 pp. (2002).
[26] Sprent, P., and Dolby, G. R., "The geometric mean functional relationship," Biometrics, 36(3), 547-550(1980).

[27] Moon, Jeong-Eon, et al. "Development of ocean environmental algorithms for Geostationary Ocean Color Imager (GOCI)." Korean Journal of Remote Sensing 26(2), 189-207 (2010) (In Korean).
[28] Lee, Z. Carder., K.L and Arnone., R.A. Deriving inherent optical properties from water color: a multiband quasi-analytical algorithm for optically deep waters "Applied Optics Vol 41. p 5755-5772 (No27 Sept 2002).
[29] Lerner, Robert M., and Hollinger, James P., "Analysis of 1.4 GHz radiometric measurements from Skylab," Remote Sensing of environment 6(4), 251-269 (1977).
[30] Schlitzer, R. "Ocean Data View," http://odv.awi.de, (2012).